Research Article

Simulation studies on picolitre volume droplets generation and trapping in T-junction microchannels

K. Sripadaraja[1] · G. Umesh[1] · M. N. Satyanarayan[1]

Received: 16 March 2020 / Accepted: 9 July 2020 / Published online: 23 July 2020

Abstract
In this paper, we present simulation studies on the formation of water microdroplets in mineral oil in a T-junction Microfluidics device. We have studied the droplet generation in two different regimes, viz., squeezing and squeezing to dripping transition regime. The effect of fluid flow rates, and surfactant concentration on the droplet generation has been investigated. It is seen that a rise in the concentration of surfactant by 4%, increases the frequency of droplet generation by 16% at the higher capillary number ($C_a = 0.02$), whereas, there is only a marginal or no change in the case of squeezing regime ($C_a = 0.0028–0.008$). We have also studied the trapping of the generated microdroplets in microwells. It is observed that the trapping of the droplet is highly influenced by the viscous drag force, droplet length, the surface energy of the droplet, droplet speed, depth of the Well for trapping and alignment of the two plates constituting the device. Our studies reveal that the droplets travelling faster than a critical trapping velocity do not get trapped in the Well. Addition of a surfactant to the mineral oil is seen to lead to a significant reduction in the critical velocity for the droplet trapping. Trapping of droplets travelling at velocities close to the critical velocity for trapping depends strongly on the alignment of the two plats of the Slip-Chip device.

Keywords Droplet microfluidics · Two phase flow · Surfactant concentration · Droplet trapping

1 Introduction

Droplet microfluidics has been intensively investigated over the last two decades due to its applications such as glucose estimation in blood [1], synthesis of micro-sized materials in monodispersed droplets [2] food quality and physiological health monitoring, polymerised chain reactions (PCR) [3], molecular-level detection [4], drug delivery [5], diagnostics in health care [6], single-cell analysis [7–9], single cell genome sequencing [10] and separation of Ca^{2+} ions from aqueous phase [11]. Droplets of picolitre volume have been of interest for single-cell analysis [12]. Multiple chemical reactions can be investigated simultaneously in a single microfluidic device by collecting microdroplets in an assay wherein very small quantities of chemicals are utilized. In all such applications, precise control of droplet size is important to produce monodisperse droplets. The three main types of devices generating droplets that are employed for experiments are Cross Junction [13], Co-flow [14] and T-junctions [15], devices. In such devices, droplet generation involves the flow of two immiscible liquids, one of which constitutes the main liquid component and is called the continuous phase, having viscosity μ_c. Much smaller quantity of the second liquid having viscosity μ_d and called the dispersed phase is injected into the main channel in which the continuous phase liquid flows. The

Electronic supplementary material The online version of this article (https://doi.org/10.1007/s42452-020-03198-9) contains supplementary material, which is available to authorized users.

✉ K. Sripadaraja, sripadaraja@gmail.com | [1]Department of Physics, National Institute of Technology, Surathkal, Mangalore, Karnataka 575025, India.

viscous shear force exerted by the continuous phase liquid on the dispersed phase liquid leads to microdroplet generation. T-junctions have been widely studied because of their simple structure and ease of analysis of droplet generation [16]. In such devices, it has been noticed that the size of the droplet and rate of its generation depends on the channel size, viscosity ratio ($\lambda = \mu_d/\mu_c$), flow rate ratio and interfacial tension between the two liquids [17]. We have investigated the generation and trapping of droplets in a T-junction type microfluidic device.

The droplets are generated in various regimes such as squeezing, transition, dripping and jetting. Capillary number (C_a) determines the regime of droplet formation. The change in capillary number was identified for different geometric aspect ratio (ratio of dispersed phase liquid to continuous phase liquid channel widths) of the device [18]. The role of fluid pressure on micro-droplet generation was revealed by pressure profiles plotted for droplet generation in squeezing, dripping and jetting regimes [19]. The details of droplet formation in squeezing to dripping-transition regime was studied to predict the droplet size and frequency of its generation and distance between the droplets [20]. This was analysed by splitting the droplet generation mechanism into three stages, viz filling stage, necking stage and lag stage. A theoretical model was proposed for the estimation of the size of droplets produced in different regimes and it was in close agreement with their experimental results. Experiments were also conducted to generate oil droplets in water using a T-junction device [21]. The droplet generation was studied for $\lambda = 0.1$, 0.03, 0.05 to understand the flow pattern, to predict the droplet size and to identify the range of C_a values at which the droplets are generated in different regimes [22]. At much higher flow rates of the dispersed phase liquid, the influence of viscous shear force gets minimised and the dispersed phase liquid flows as a separate stream parallel to the continuous phase liquid in the main channel. Hence, for droplet generation fluid flow ratio is restricted to $Q_d/Q_c < 0.3–0.5$. A novel geometry with a spiral microchannel was used to demonstrate extraction of calcium metal ions from aqueous phase [23]. These studies on T-junction, have revealed the role of the capillary number, viscosity ratio, flowrate of the two fluids and the ratio of width of the two channels on droplet generation.

The interfacial tension between the two immiscible liquids and the contact angle of the droplet with the surface of the flow channel are two important factors that contribute to droplet generation. In practical applications, the droplets generated are collected in a vial for further investigations. Further, the droplets of interest are pipetted out manually. To prevent droplets from coalescing in the vial, surfactants are added to one of the two liquids based on their solubility. This reduces the interfacial tension [24]. This in turn, reduces the pressure difference ΔP [Pressure in dispersed phase liquid—Pressure in the continuous phase liquid]. Besides, the rate of droplet generation will also increase to maintain the mass flow to be constant. Consequently, there is a reduction in droplet size and an increase in the frequency of droplet generation [25]. Bashir et al. [27] showed that the role of contact angle and interfacial tension on the droplet is more significant for the viscosity ratio of 0.8 than for 0.1. The length of the droplet is higher for $\lambda = 0.8$ than for $\lambda = 0.1$ for a fixed flow-rate ratio and interfacial tension. The pinch-off time of the droplet decreases as there is an increase in contact angle from 120° to 180°. The interfacial tension was evaluated for silicone oil having four different viscosities (10 cSt, 20 cSt, 50 cSt, 100 cSt) with two different dispersed phase media (Deionised water and FC43) [28]. In the experiments performed, it was observed that the droplet length remained almost the same over a range of capillary number from 0.0028 to 0.008. Using the traditional volume of fluid method, the change in interfacial tension by addition of nanoparticles of sizes varying from 10 nm to 100 nm and its effect on droplet generation was studied [29]. The droplet size was seen to get reduced with increase in the concentration of nanoparticles. The effect of concentration of surfactants like SDS (sodium dodecyl sulphate) or Tween 20 added to silicone oil has been experimentally studied wherein the interfacial tension was evaluated by recording the droplet generation using a high-speed camera [30]. Further based on their study an analytical model was formulated to determine the interfacial tension due to increased surfactant concentration. Most of these experimental studies consider uniform distribution of surfactant molecules at the droplet interface and focus on the influence of surfactant and its increasing concentration on both size and frequency of droplet generation in various regimes. Numerical simulations can help identify the influence of surfactant concentration at the droplet/bubble interface [31]. The influence of surfactant (Span 80 mixed with octane) on droplet generation was numerically investigated using Lattice Boltzmann Method [32]. This study uses two computational models to present uniform and non-uniform distribution of surfactant at the interface. The model adopted for non-uniform distribution of surfactant explains the droplet generation mechanism which was experimentally demonstrated [33]. The surfactant adsorption first appears at the front end of the droplet as it expands into the main channel and gradually covers the entire droplet before it is released. The velocity vectors profile inside the droplet indicates liquid circulation which vanishes as the droplet is about to be released. It is also observed that the frequency of droplet generation increases for capillary number ranging from 0.01 to 0.1. Recently such increase in frequency was also

demonstrated using numerical simulation [26]. In our 2D simulation, we study how the surfactant (Span 80) concentration influences droplet generation for C_a ranging from 0.0028–0.02. For low values of C_a the droplet generation occurs due to squeezing process and for C_a values close to 0.01 the transition to dripping regime begins. We have also investigated the influence of surfactant on the frequency of droplet generation and its size in squeezing regime and the transition regime, which were not reported by Bashir et al. [45].

To capture individual microdroplets for further analysis, trapping of generated droplets in an array of microwells is convenient. We have investigated droplet generation and trapping in Slip-Chip type device in the T-junction geometry. This device consists of two separate plates, one having cylindrical Well and the second plate having a shallow Pit with circular opening along the main channel. The second plate is placed on the plate containing the Wells such that the Pit lies over the Well. Different mechanisms exploited for trapping involve manipulation of surface energy [34], hydrodynamic based trapping [35] and Laplace pressure [36]. Surface energy-based trapping is achieved by proper choice of the geometry of the device and the micro-wells [34, 37]. In these studies, the volume of the Well was taken to be smaller than the droplet volume and hence, the entire droplet cannot get into the Well. A droplet moving towards the Well experiences a force proportional to the gradient of surface energy which arises due to the deformation of the droplet as it enters the Well. When the hydrodynamic drag force is less than the force due to surface energy gradient, the droplet gets anchored to the Well and partially enters the Well. The effect of surface energy change leading to trapping was numerically studied [38]. Further, the change in Laplace pressure of droplet entering the Well was also determined. It was seen that an increase in the flow rate of the continuous phase liquid, resulted in non-trapping of the droplet or if the droplet is anchored, it detaches leaving a small fragment, called the daughter droplet, trapped inside the Well. The critical capillary number at which droplet anchoring happens was determined for different viscous media [39]. The anchoring of droplet to microwell was studied using Lattice Boltzmann Method [40]. This study demonstrates that the anchoring efficiency increases with increase in the diameter of the well.

In this paper, we have studied the formation of microdroplets of water in mineral oil (density $\rho = 840$ Kg/m^3 and viscosity $\mu = 24.1$ mPa-s). We have studied the dependence of microdroplet length on the surfactant concentration (Span 80). We have also investigated the impact of surfactant on the frequency of droplet generation and its size in squeezing and transition regimes by examining the pressure versus time plots at point P_c and P_d shown in Fig. 2. These graphs reveal that the pressure within the two immiscible liquids reduces with an increase in surfactant concentration. It is also seen that the frequency of droplet generation increases for increased surfactant concentration in the transition regime but not in the squeezing regime. We demonstrate that elongated droplets (confined due to the geometry of the channel) can be trapped inside the well due to surface energy change. We show that the trapping of droplet occurs at the velocity (U_c) which is less than the critical velocity (U_{cr}) depending on its size and Well depth.

2 Microfluidic device model

The T-junction device in the model Slip-Chip configuration is schematically shown in Fig. 1a. The channels for liquid flow have rectangular cross-section of width of 100 µm and depth of 50 µm. In this device, the channel plate is on top and the Well plate is at the bottom with the channel and the well facing each other. The continuous phase liquid used is mineral oil and it flows into the device through the "main channel" inlet. The dispersed phase liquid is water, which flows into the junction through the "side channel" inlet. The droplets of water, generated at the junction, move down-stream along with the oil (Fig. 1b). The shear force of the viscous oil medium on water and the interfacial tension between them govern the release of the droplet of water at the junction. Simulations were done using ANSYS Fluent software v18.1. A numerical method combining the Level Set method (LSM) and Volume of fluid model (VOF) has advantages over just VOF for analysing the model [41]. We have adopted this combined model in our simulation study.

Simulation of both, the droplet generation and its trapping together require large computation time. Hence, we study the trapping mechanism separately by employing a 3D model. We observe that the droplet moves in the channel along with the continuous phase liquid. A typical microfluidic device comprises of two plates, one with the channel and the other having the Wells. The two plates are bonded one over the other to create the device. In the case of a SlipChip [42] device, the two plates are sealed with a temporary sealing. The lower plate, called Well Plate, has a cylindrical Well of diameter 200 µm and depth 200 µm for most of our simulations. The upper plate, called Channel Plate, has the T-shaped channel, for liquid flow, and a shallow Pit, with circular opening, located well away from the T-junction. The Pit has a diameter of 200 µm and depth of 50 µm. The broadside and top view of the device is shown in Fig. 1a, b, respectively. It is observed that the Pit in the Channel plate influences trapping of droplets in the Well in the Well plate as explained below in Sect. 4.

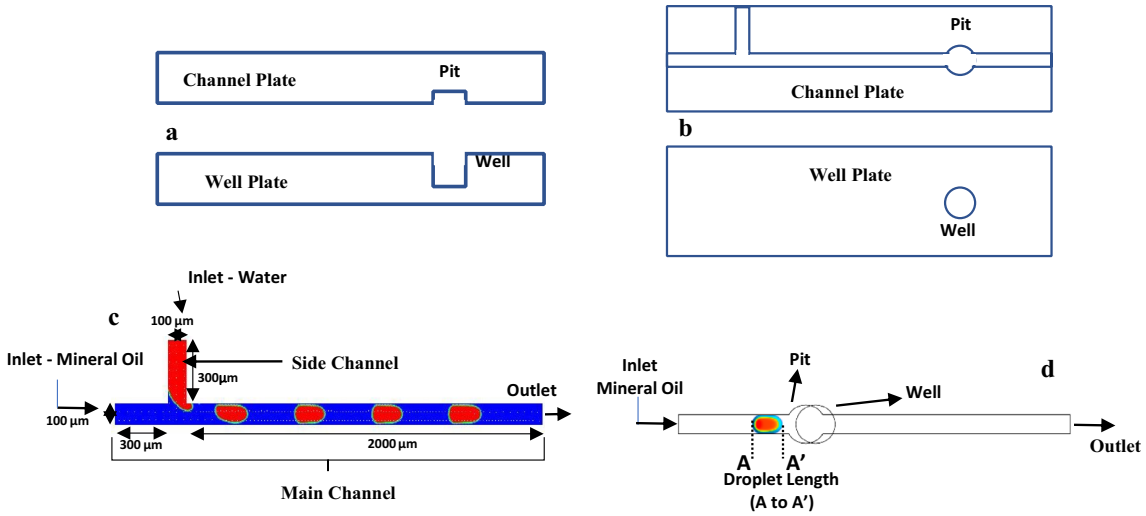

Fig. 1 Schematic of the Slip Chip Microfluidic device showing the Well, the Pit and the channel for liquid flow; **a** broadside and **b** top view; **c** 2-D geometry for simulation of droplet generation; **d** schematic for droplet trapping for 75% alignment of the Pit with the Well

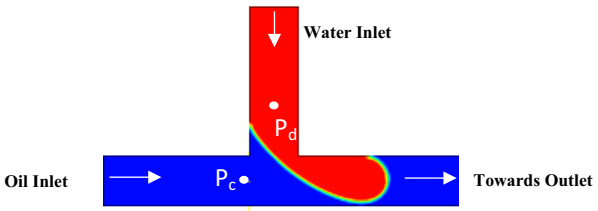

Fig. 2 Location of pressure measuring points P_d and P_c in dispersed phase and continuous phase liquids respectively

The basic equations used in the simulation are listed below. The continuity equation for an incompressible fluid is given by [43]

$$\nabla . \left(\rho_{avg}\overrightarrow{U'}\right) = 0 \tag{1}$$

And the Navier–Stokes equation of motion for the fluid is given by,

$$\frac{\partial\left(\rho_{avg}\overrightarrow{U'}\right)}{\partial t} + \nabla \cdot \left(\rho_{avg}\overrightarrow{U'U'}\right) = -\nabla P + \nabla\cdot\overline{\tau} + \vec{F} \tag{2}$$

where $\overrightarrow{U'}$, P, ρ_{avg} and $\overline{\tau}$ are velocity, pressure, density (averaged), and stress tensor respectively for the fluid. For Newtonian liquids which are incompressible, the shear stress is relative and proportional to the rate of strain tensor γ which is represented as,

$$\overline{\tau} = \gamma\eta_{avg} = \eta_{avg}(\nabla\overrightarrow{U'} + \nabla\overrightarrow{U'^{*}}) \tag{3}$$

where η_{avg} is the averaged viscosity. For the two-component fluid being considered, we define the density and viscosity of the volume (averaged) in-terms of the fractional volume of the two immiscible fluids such as oil (V_o) and water (V_w) as follows [43].

$$\rho_{avg} = V_0\rho_o + \left(1 - V_w\right)\rho_w \tag{4}$$

$$\eta_{avg} = V_0\eta_o + \left(1 - V_w\right)\eta_w \tag{5}$$

The fractional volume of the individual fluid phase is computed by resolving the following equation

$$\frac{\partial V_f}{\partial t} + \overrightarrow{U'}\cdot\nabla V_f = 0 \tag{6}$$

"f" is the subscript that describes any of the two fluids. In each mesh element, the fractional volume of the two phases is conserved implying $\Sigma V_f = 1$. If $V_f = 0$, the specific mesh element is said to be empty of the 5th phase and $V_f = 1$ indicating that the element (cell) is loaded with the 5th phase. Thus, the two-phase interface is demarcated by the value of the fractional volume.

We adopt the model of continuum surface force (CSF) and accordingly define the interfacial tension force ($\overrightarrow{F'}$) which is volumetric and is represented as

$$\overrightarrow{F'} = \sigma\left(\frac{\rho R_n\nabla V_0}{0.5\left(\rho_0 + \rho_\omega\right)}\right) \tag{7}$$

where "σ" is the coefficient of interfacial tension among two liquids and R_n the radius of curvature of the droplet is expressed in terms as

$$R_n = -\nabla \cdot \hat{n} = \frac{1}{|\vec{n}|}\left[\left(\frac{\vec{n}}{|\vec{n}|} \cdot \nabla\right)|\vec{n}| - (\nabla \cdot \vec{n})\right] \quad (8)$$

where $\hat{n}$ is the component normal to the droplet surface. Considering the formulation VOF the surface normal $|\vec{n}|$ is expressed as the gradient of fractional volume phase at the interface which can be written as

$$\vec{n} = \nabla V_f \quad (9)$$

The force due to interfacial tension is implemented by piecewise linear interface calculation [43, 44]. The change in the interfacial tension in our study is due to increased surfactant concentration. Hence the convection–diffusion equation is considered, which is given by [31],

$$\frac{\partial \alpha}{\partial t} + \vec{\nabla} \cdot \left(\overrightarrow{U'}\alpha\right) = \vec{\nabla} \cdot \left(D_c \vec{\nabla}\alpha\right) \quad (10)$$

where α is the surfactant concentration in the bulk fluid and D_c is the diffusion coefficient of surfactant in bulk liquid.

The effects of wall adhesion are considered by providing the necessary value for the contact angle with the channel wall (Θ_w). Therefore, the surface normal at the reference cell next to the wall is given by,

$$\hat{n} = \hat{n}_w \cos\theta_w + \hat{m}_w \sin\theta_w \quad (11)$$

where $\hat{n}_w$ and $\hat{m}_w$ are the unit vectors which are normal and tangential to the wall respectively.

3 Simulation sequence

3.1 Model for simulation using VOF solver

We have used ANSYS Fluent solver "Pressure Implicit with Splitting of Operators (PISO)", for simulating the droplet generation taking account of the coupling between pressure and velocity in the momentum equation. Any false currents which may arise because of mismatch between the pressure and interfacial tension forces are removed using the Pressure staggering option (PRESTO). We adopt the implicit method of the first order for the discretization of derivatives with time. The convergence criterion for solution of the continuity equation, the equations for X-momentum and Y-momentum, and the computation of the Level Set function was set as a residual of 0.001. Thus, if the residual in any computation drops below 0.001, then the solution is treated as having converged. Accordingly, we set the flow time to be 0.5 sec with a step size of 10 μSec. The global Courant number, which is a dimensionless quantity is maintained less than 0.2; it varied between 0.08 to 0.17 throughout the simulation. This relates the time step increment and its duration in the transport equations to the distinctive time of transportation of the fluid element across a control volume. The flow rate of the two liquids is prescribed at the respective inlets and normal outflow condition is prescribed at the common outlet. The resultant droplet length is noted. Simulation is performed assuming that the inner surface of the channel is oleophilic and hence is completely wetted by the continuous phase liquid. We consider no-slip boundary condition for the continuous phase liquid. We take into account the effects due to the addition of surfactant in the simulation study by varying both interfacial tension and contact angle in the range 7 mN/m to 4 mN/m and 152° to 172° respectively [45]. Hexahedral mesh with an element size of 2 μm is adopted for all the 2D simulation. The mesh convergence analysis was done to achieve a residual level less than 0.001 as mentioned above. We carried out simulations to determine droplet length taking mesh elements of size 4 μm, 2 μm and 1 μm. It was seen that the difference in droplet length for a mesh size of 2 μm as against 1 μm was less than 0.001. Hence, all the simulations were carried out for mesh elements of size 2 μm which corresponded totally to about 130,000 elements. The main channel length is kept sufficiently long for the flow to become fully developed.

3.2 Analysis of droplet generation by 2D simulation

2D simulations were performed to understand the influence of surfactant concentration in generating droplets. In a T-junction device (Fig. 1c), the continuous phase liquid (Mineral oil – density $\rho = 840$ Kg/m^3 and viscosity $\eta = 24.1$ mPa-s) and the dispersed phase liquid, (Water–density $\rho = 998$ Kg/m^3 and viscosity $\eta = 1$ mPa-s) are let in through two different inlets. The dispersed phase liquid, shown in red color enters through the side channel and creates an interface with the continuous phase liquid, which is shown in blue color, at the junction. Span 80 was chosen as the surfactant for our investigations.

The surfactant concentration, in terms of the ratio of the weight of Span-80 to that of Mineral Oil, was kept at 0.2%, 0.4%, 0.8%, 1%, 2%, 3% and 4%. Droplet generation is studied for various flow rate Q_c of oil, the continuous phase liquid. We have taken contact angle data for our simulations from past experimental data [45]. The pressure profiles at points P_c and P_d (Fig. 2) are computed for various surfactant concentrations to correlate it with the droplet length and droplet release time.

3.3 Analysis of droplet trapping by 3D simulation

3D Simulations were performed to analyse microdroplet trapping as shown in Fig. 1d. Once the water droplet is released, it is under the influence of the continuous phase liquid and moves downstream along with the oil. During the trapping process the droplet shape changes but its volume remains constant. Change in the droplet shape implies change in surface energy of the droplet. The trapped droplet assumes a shape corresponding to minimum surface energy. In the simulation we have monitored the dynamic change in the droplet shape to get a better understanding of the trapping conditions [34].

The droplet length depends on the flow rate ratio of the two liquids. In our studies, the droplet length ranged from 70 µm to 200 µm. This compares well with previous experimental data [45]. Hence, for trapping studies, we consider droplets of length 200 µm, 100 µm, and 50 µm (A-A') in shown in Fig. 1d. It is seen that beyond a certain velocity the droplets do not get trapped. We define the maximum droplet velocity at which the trapping happens as the critical trapping velocity. In addition to droplet length, we have also investigated the dependence of trapping on the Well depth (200 µm, 150 µm, and 50 µm) and the alignment of the two plates of the Slip-Chip device.

In the 3D simulation, the velocity U_c of the continuous phase liquid was initially set to 1 mm/s. The droplet is transported by the continuous phase liquid and thus has the same velocity U_c. Simulations were repeated for increasing values of U_c until the critical trapping velocity is reached. Normal outflow boundary conditions were set at the outlet. The simulations were repeated for different Well alignments (100%, 75%, 50%, 25%, 0%) with the channel plate as shown in Fig. 6a–e.

4 Results and discussion

4.1 Effect of surfactant on droplet generation

The droplet formation process is illustrated in Fig. 3. When the dispersed phase liquid (water) enters the main channel, it progressively blocks the flow of the continuous phase liquid (Oil) leading to an increase in the pressure at point P_c (Fig. 2). It reaches a peak value and decreases sharply to a very low value which indicates the release of one droplet (Fig. 3d–f). This process repeats periodically leading to generation of multiple droplets at a definite frequency. It has been shown that at low liquid flow rates, the droplet generation occurs due to the Squeezing

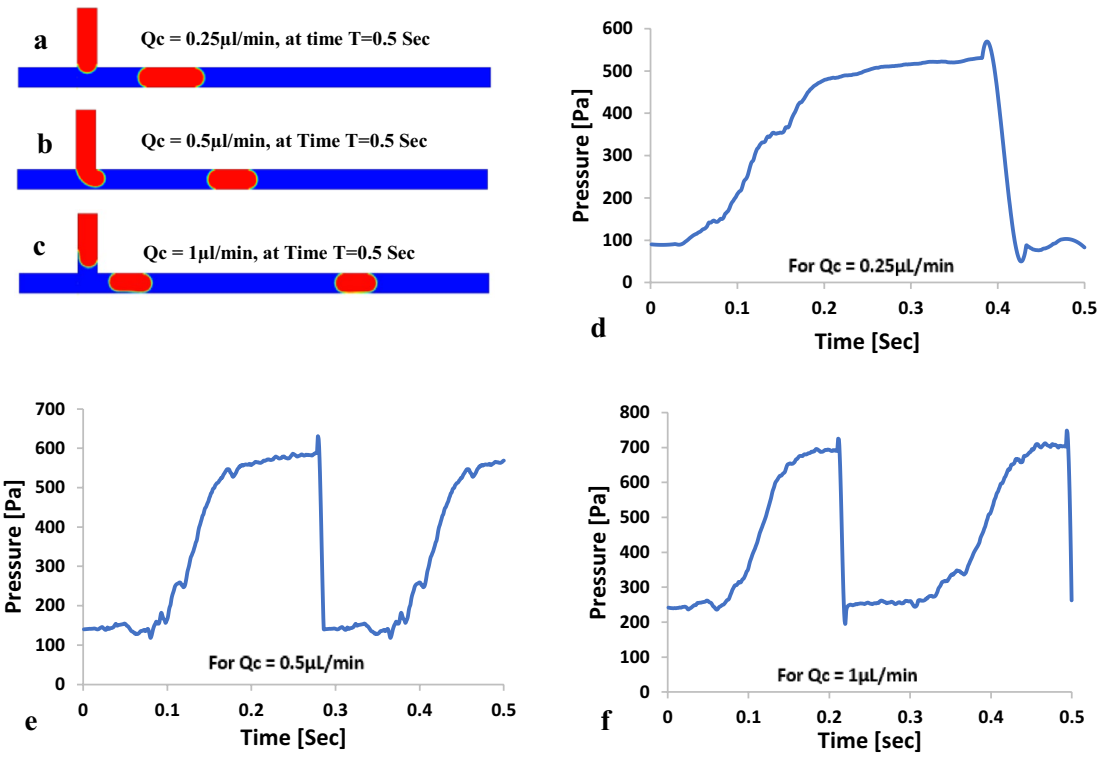

Fig. 3 Droplet generation for different flowrate of continuous phase liquid without the surfactant at fixed value of $Q_d = 0.2$ µl/min. **a** $Q_c = 0.25$µL/min. **b** $Q_c = 0.5$µL/min **c** $Q_c = 1$µL/min, **d**–**f** Pressure versus time at point P_c for Q_c values as in a-c respectively

mechanism and at somewhat higher flowrates the generation occurs due to Dripping mechanism [46]. There is a gradual transition from Squeezing regime to Dripping regime as the flow rates are increased. We have investigated droplet generation in the transition regime also by simulation. Each simulation is carried out for a total fluid flow duration of 0.5 s.

The interfacial tension between mineral oil and water is taken to be 24.5 mN/m [47] in the absence of surfactant. Droplets of lengths 296 µm, 228 µm and 192 µm are generated in the squeezing regime as shown in Fig. 3a–c, for a fixed $Q_d = 0.2$ µL/min and $Q_c = 0.25$ µl/min, 0.5 µl/min and 1 µL/min, respectively. At these flow rates, the time variation of pressure at point P_c is shown in Fig. 3d–f and it is seen to reach a peak value of 526 Pa, 573 Pa and 690 Pa for the different Q_c values. The rise time T_R of the pressure profile is estimated to be 0.115 sec, 0.072 sec, and 0.067 sec for the flowrate values $Q_c = 0.25$ µL/min, 0.5 µL/min and 1 µL/min, respectively. The corresponding fall time T_F for all flowrates was found to be about 0.003 sec. The long rise time indicates a slow initial growth of the droplet and the much smaller fall time implies a very quick pinch-off leading to the release of the droplet. Figure 3c shows that at higher flow rates of Q_c, the droplet generation frequency increases. The pressure at point P_c attains a peak value just prior to the release of the droplet. In general, the pressure at point P_c increases with increase in the flowrate Q_c [48, 49]

The addition of a surfactant has been shown to alter the droplet size and the droplet frequency [50]. Figure 4 shows the droplet generation using oil (continuous phase liquid) containing surfactant with concentrations varying from 0.2% to 4% by weight for different values of Q_c, keeping Q_d fixed at 0.2 µl/min. Figure 4a shows droplet for flowrate $Q_c = 1$ µl/min for different surfactant concentrations.

At this flowrate, the addition of a surfactant results in a reduction of the maximum pressure at point P_c from 690 Pa to 352 Pa for a surfactant concentration of 0.2%, which further reduces to 329 Pa when concentration is increased to 4% (Fig. 4d). Similar trend is seen for $Q_c = 0.5$ µl/min and 0.25 µl/min as evident from 4(f&h). The pressure at point P_d also shows similar reduction as the concentration increases from 0.2% to 4% (Fig. 4g and i). We may also conclude from Fig. 4 that with increasing surfactant concentration the droplet length decreases monotonically and the droplet generation frequency increases. Figure 4d–l also indicate that the droplet generation frequency increases as the flowrate of Q_c increases. Further, it is seen that the rise time of the pressure profile at point P_d is much shorter than that for the pressure profile at point P_c, whereas the fall time is practically the same for both cases. This indicates that the dispersed phase liquid relaxes to its initial state very fast after the droplet is released. The plateau in the pressure profiles is longer for the pressure plots at point P_d compared to that for the plots at point P_c. The duration corresponding to the plateau in the pressure plots at point P_d may be taken to be the duration required for the formation of the droplet as shown in Table 1 below. The results of the pressure change are summarised in Table 2.

The droplets were generated for a fixed value of $Q_d = 0.2$ µL/min and varying $Qc = 0.2$ µL/min to 2 µL/min. This study was repeated for surfactant concentration ranging from 0% to 4%. The droplet length reduces significantly for low Q_c values and acquires a minimum value as Q_c increases to higher values as shown in Fig. 5a. The variation of L/w, the dimensionless droplet length, with the flowrate ratio Q_d/Q_c is shown in Fig. 5b. The linear scaling of L/w with flowrate ratio is specific to the range $0.01 < Q_d/Q_c < 0.1$ [46].

We have computed the surfactant concentration profile at the droplet interface. The surface density of the surfactant is higher at the two poles of the droplet than at the flat parts adjacent to the channel walls. It is a little higher at the front pole of the droplet as compared to that at the rear which is in confirmation with the results of Riaud et al. [32]. The variation of the surfactant concentration at the front pole of the droplet is shown in Fig. 5c–f, for bulk surfactant concentration of 0.2%, 1% and 4%.

Clearly, the entire droplet surface is covered by a thin layer of surfactant molecules since the adsorption of these molecules is much faster than the droplet formation time. Once the droplet is released, it is seen to conserve its volume and shape till it reaches the Well where it may be trapped. The presence of surfactant is seen to influence the trapping of the droplet.

4.2 Droplet trapping

After its release at the T-junction, a droplet acquires an elongated pancake shape due to the rectangular cross-section of the main channel in our device; we shall call such a droplet as a "Plug". The surface energy of the droplet is given by $E = \gamma A$, where γ is the interfacial tension and A is the surface area of the droplet. Since the Plug is not spherical in shape, its surface energy is larger. As the droplet enters the Well, meant for trapping it, the droplet encounters the Well as well as the Pit in the two plates of the device. Here the droplet spreads into the circular Well and the Pit and acquires a shape such that its surface energy reduces. This change in surface energy over the spatial region of the Well leads to an attractive force on the droplet proportional to the gradient of the surface energy. This mechanism is shown to be responsible for the trapping of the droplet [34]. We have studied the trapping of microdroplet into the well for different flow rates Q_c in

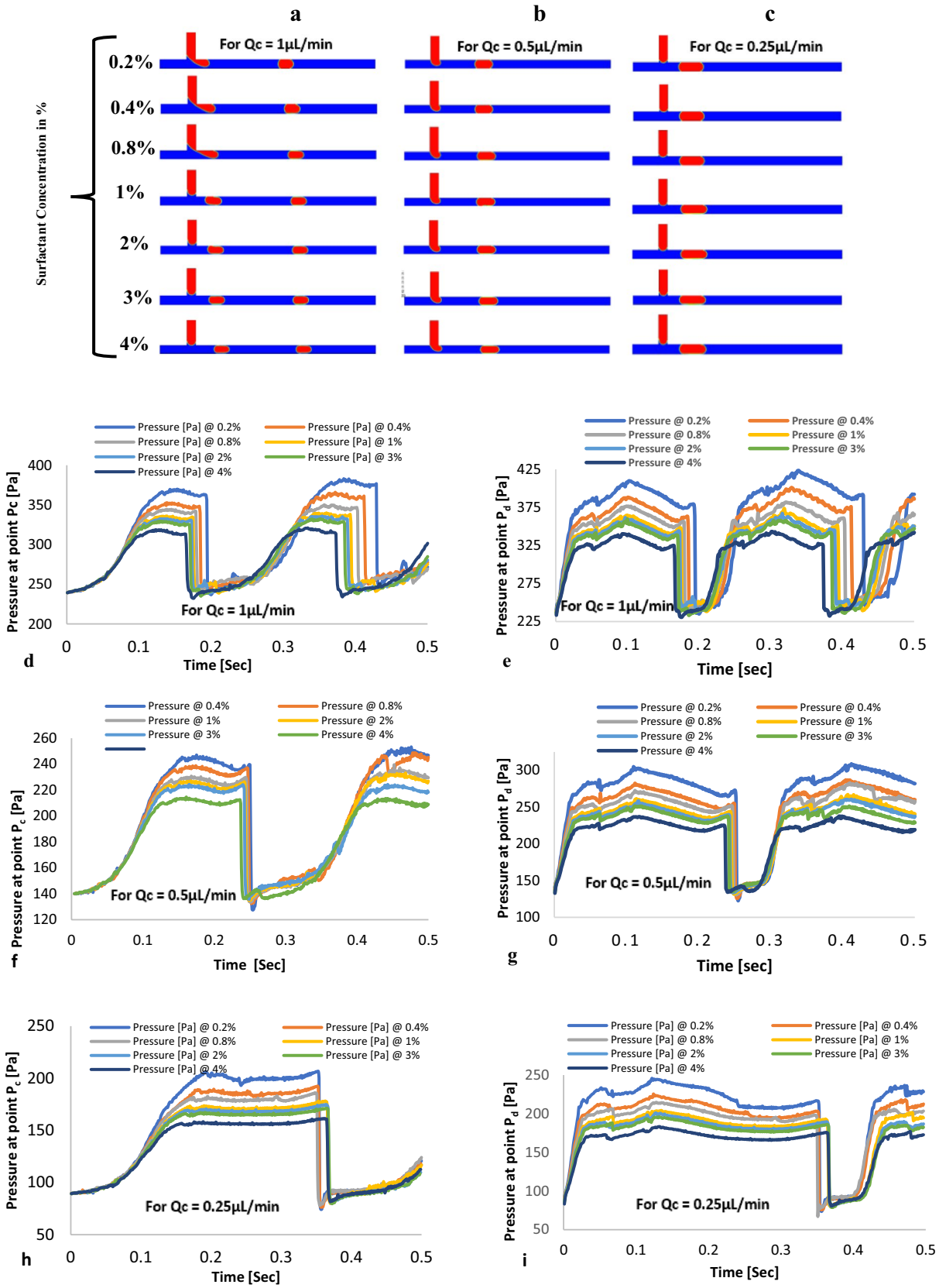
a
b
c
For Qc = 1µL/min
For Qc = 0.5µL/min
For Qc = 0.25µL/min
Surfactant Concentration in %
0.2%
0.4%
0.8%
1%
2%
3%
4%
Pressure [Pa] @ 0.2%
Pressure [Pa] @ 0.4%
Pressure [Pa] @ 0.8%
Pressure [Pa] @ 1%
Pressure [Pa] @ 2%
Pressure [Pa] @ 3%
Pressure [Pa] @ 4%
Pressure at point Pc [Pa]
For Qc = 1µL/min
Time [Sec]
d
Pressure @ 0.2%
Pressure @ 0.4%
Pressure @ 0.8%
Pressure @ 1%
Pressure @ 2%
Pressure @ 3%
Pressure @ 4%
Pressure at point Pd [Pa]
For Qc = 1µL/min
Time [sec]
e
Pressure @ 0.4%
Pressure @ 0.8%
Pressure @ 1%
Pressure @ 2%
Pressure @ 3%
Pressure @ 4%
Pressure at point Pc [Pa]
For Qc = 0.5µL/min
Time [Sec]
f
Pressure @ 0.2%
Pressure @ 0.4%
Pressure @ 0.8%
Pressure @ 1%
Pressure @ 2%
Pressure @ 3%
Pressure @ 4%
Pressure at point Pd [Pa]
For Qc = 0.5µL/min
Time [sec]
g
Pressure [Pa] @ 0.2%
Pressure [Pa] @ 0.4%
Pressure [Pa] @ 0.8%
Pressure [Pa] @ 1%
Pressure [Pa] @ 2%
Pressure [Pa] @ 3%
Pressure [Pa] @ 4%
Pressure at point Pc [Pa]
For Qc = 0.25µL/min
Time [Sec]
h
Pressure [Pa] @ 0.2%
Pressure [Pa] @ 0.4%
Pressure [Pa] @ 0.8%
Pressure [Pa] @ 1%
Pressure [Pa] @ 2%
Pressure [Pa] @ 3%
Pressure [Pa] @ 4%
Pressure at point Pd [Pa]
For Qc = 0.25µL/min
Time [Sec]
i

◂**Fig. 4** Droplet generation sequence and pressure versus time plots for various surfactant concentration (weight %) at a fixed value of Q_d at 0.2 µl/min and changing Q_c **a** $Q_c = 1$µL/min. **b** $Q_c = 0.5$µL/min **c** $Q_c = 0.25$µL/min, for a total flow time of 0.5 Sec.; Pressure versus time at point P_c and P_d respectively for **d**, **e** $Q_c = 1$µL/min; **f**, **g** $Q_c = 0.5$µL/min and **h**, **i** $Q_c = 0.25$µL/min

the presence of surfactants. The droplets experience lower shear stress in the region where the Well is located [51]. We have studied trapping of droplets of different lengths (200 µm and 100 µm) in the Well under the influence of the pit. To understand the trapping mechanism better we have varied the diameter of the pit, its alignment with the Well and the depth of the Well in the simulations.

Figure 6a–e shows the alignment of the Well and the Pit. Figure 6f, g illustrates the top view and the side view of the device geometry adopted for the simulations.

Figure 7 shows the change in the shape of the droplet (plugs) of different lengths due to the Pit as they get close to the Well. For the different extent of alignment between the Well and the Pit, as shown in Fig. 6a–e, the change in the shape of the droplets is more for larger alignment. This change in shape is such that the surface energy of the droplet gets reduced and this contributes to the trapping of the droplet in the Well. In these simulations the diameters of the Well and the Pit are both taken as 200 µm.

In the case of droplet length 200 µm, we have investigated the trapping of droplets for different Pit diameter keeping the Well diameter as 200 µm, Well depth as 200 µm and for perfect alignment of the Pit with the Well. We varied the diameter of the Pit from 200 µm to 20 µm, the flow velocity U_c of oil from 3 mm/s to 10 mm/s and the bulk surfactant concentration in oil was kept 4%. Our simulations reveal that the droplet is trapped in the Well only if the flow velocity U_c is less than a critical value U_{cr}. The droplet becomes spheroidal in shape as it gets into the Well and its surface energy is also lowered. Thus, we conclude that when the flow velocity exceeds U_{cr} the viscous drag force on the droplet overcomes the force due to surface energy gradient, which anchors it to the Well. Consequently, the droplet gets out of the Well and moves downstream with the oil. The value of U_{cr} is seen to depend on the bulk surfactant concentration. For a Pit diameter in the range 20 µm to 100 µm and surfactant concentration of 4%, the droplet is seen to get trapped in the Well for oil flow velocity $U_c < U_{cr} \sim 4.5$ mm/s and at a higher flow velocity it escapes from the Well. The simulations also reveal that, before the droplet moves out of the Well, a few tiny water droplets break away from it and move downstream. When the Pit diameter is increased beyond 100 µm (the width of the channel) the critical velocity increases to ~ 7.3 mm/s. This may be ascribed to the change in the geometry of the Well-Pit combination in the device for Pit diameter > 100 µm. Without surfactant the critical velocity is seen to be > 15 mm/s. Thus, surfactants cause a significant reduction in the critical velocity for trapping.

Table 1 Droplet release time based on flowrate of oil (Q_c) at fixed Qd = 0.2µL/min

Flow rate Q_c	0.2 µL/min	0.5 µL/min	1 µL/min
Droplet formation time	0.35 s	0.17 s	0.08 s

The trapping of droplets is seen to depend on the depth of the Well. To study this aspect we carried out simulations on droplet trapping for Well depth ranging from 200 µm to 50 µm keeping the flow velocity U_c constant at 4 mm/s and Well and Pit diameter at 200 µm. The alignment of the Well and the Pit was kept at 100% and 50%. Droplet trapping occurred only if the Well depth was above 100 µm irrespective of the Well-Pit alignment. We also studied the role of the alignment of the Well with the Pit, keeping the Well and Pit diameter and the Well depth at 200 µm. For flow velocities $U_c < U_{cr}$ the droplets are invariably trapped, but for higher flow velocities the droplets do not get trapped irrespective of the extent of alignment. For flow velocity of oil $U_c = 7$ mm/s which is close to $U_{cr} \sim 7.3$ mm/s, the simulations reveal that the droplet gets trapped if the Well-Pit alignment is < 50% and does not get trapped for alignment > 80%. For alignment between 50 and 80%, the droplet is just trapped and several small daughter droplets break off from the main droplet and travel downstream. This confirms the conclusion that, close to the critical velocity for droplet trapping, the escape of the droplet from the Well is preceded by generation of several tiny daughter droplets.

In the case of droplet length of 100 µm, U_c is varied between 1 mm/sec to 12 mm/s. The droplet experience lesser drag force (as compared to droplet length 200 µm) due to the reduced surface area for different Pit-Well alignment. The change in the surface area is shown in Fig. 7i–m. The reduced surface energy shows that the droplet is trapped if U_c is less than 1.3 mm/s, 5 mm/s, 6 mm/s and 10 mm/s for Pit-well alignment of 100%, 75%, 50% and 25% respectively when the Well depth is 200 µm. This reduces to 3 mm/s, 5 mm/s, and 6 mm/s for alignment of 75%, 50% and 25% respectively when the well depth reduces to 150 µm.

4.3 Comparison of simulation results with past experiments

Our simulation study is validated with an experimental study done by Bashir et al. [45] for a surfactant concentration at 4%. The properties of liquids, the channel dimensions, and the flowrates of the two liquids are maintained

Table 2 Effect of surfactant concentration on droplet length and maximum pressure at point P_d and P_c

Flowrate ratio Qc	No surfactant			Surfactant concentration 0.2%			Surfactant concentration 4%		
	Droplet Length in µm	Pressure at P_c in [Pa]	Pressure at P_d in [Pa]	Droplet Length in [µm]	Pressure at P_c in [Pa]	Pressure at P_d in [Pa]	Droplet Length in [µm]	Pressure at P_c in [Pa]	Pressure at P_d in [Pa]
1 µl/min	192	690	820	160	352	393	148	329	322
0.5 µl/min	228	573	690	200	237	282	196	218	220
0.25 µl/min	296	526	610	268	199	208	268	155	166

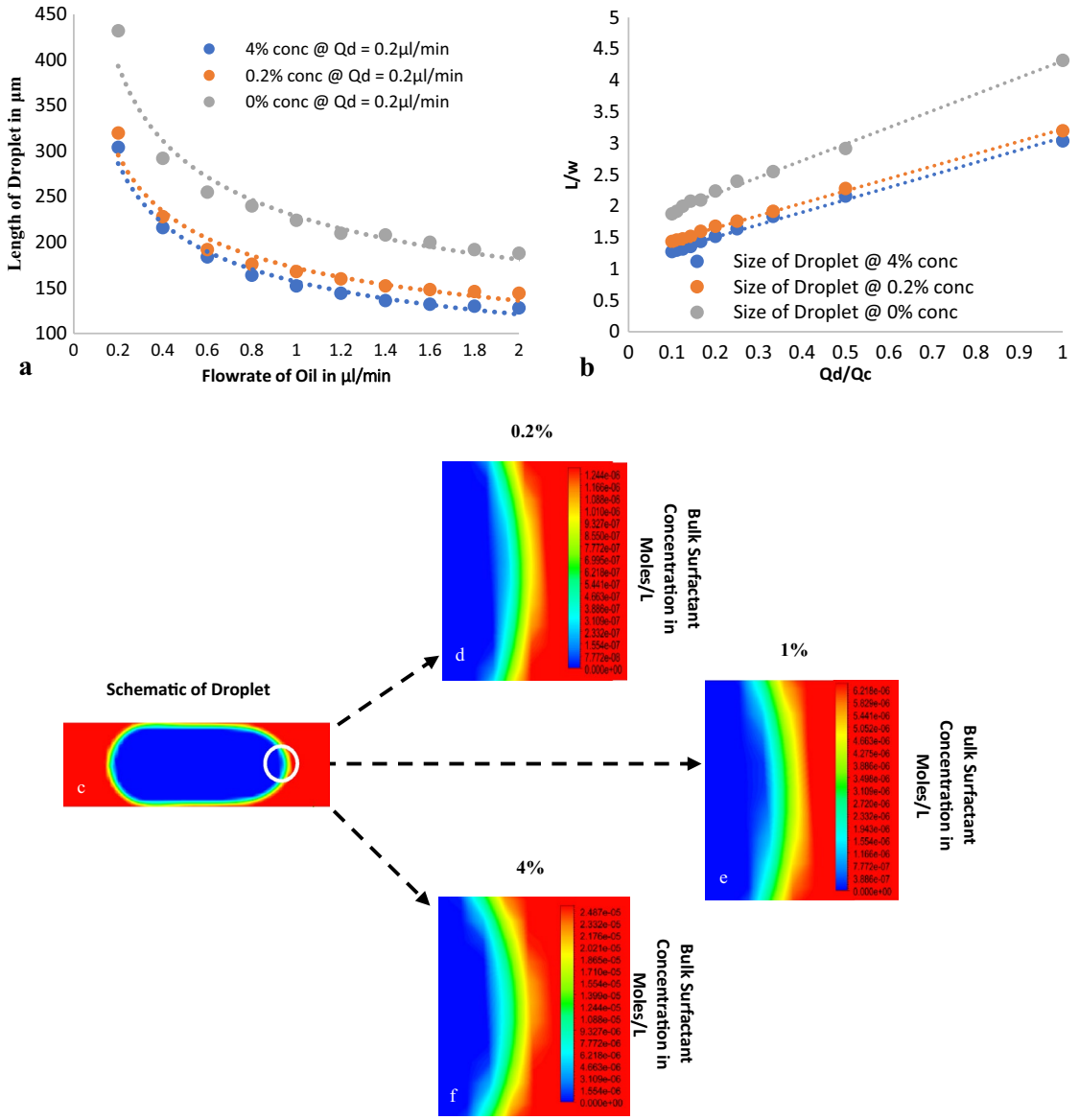

Fig. 5 **a** Droplet length versus flowrate of oil (for fixed $Q_d = 0.2$ µl/min). **b** Dimensionless droplet length (L/w) versus flowrate ratio. **c** Surfactant concentration profile (in moles/litre) at the front pole of the droplet (oil is shown in red and water is shown in Blue colour). **d–f** interface of the droplet for concentration 0.2%, 1% and 4% respectively

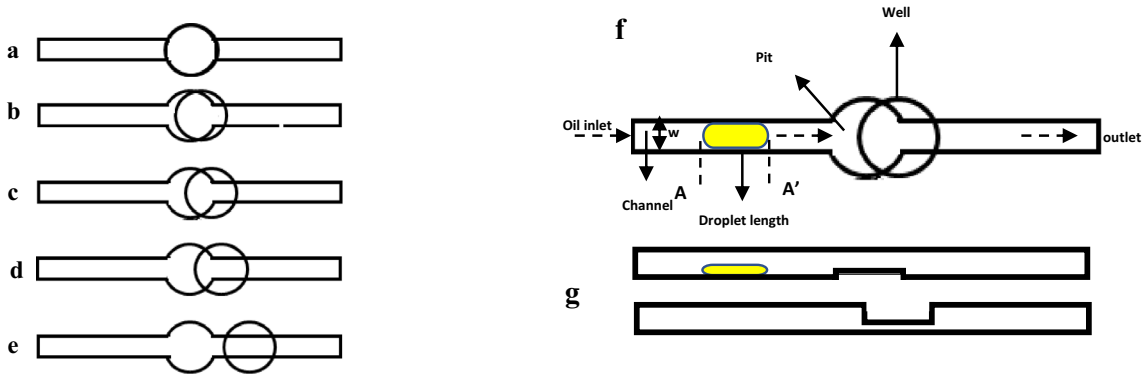

Fig. 6 **a** Top view of the microchannel geometry with the Well shown as a full circle and the Pit with the channel. The different extents of alignment of the Well and the Pit are **a** 100% alignment **b** 75% alignment **c** 50% alignment **d** 25% alignment and **e** total mis-alignment; **f** Top view of the droplet in the channel; **g** Broadside view of the droplet in the channel

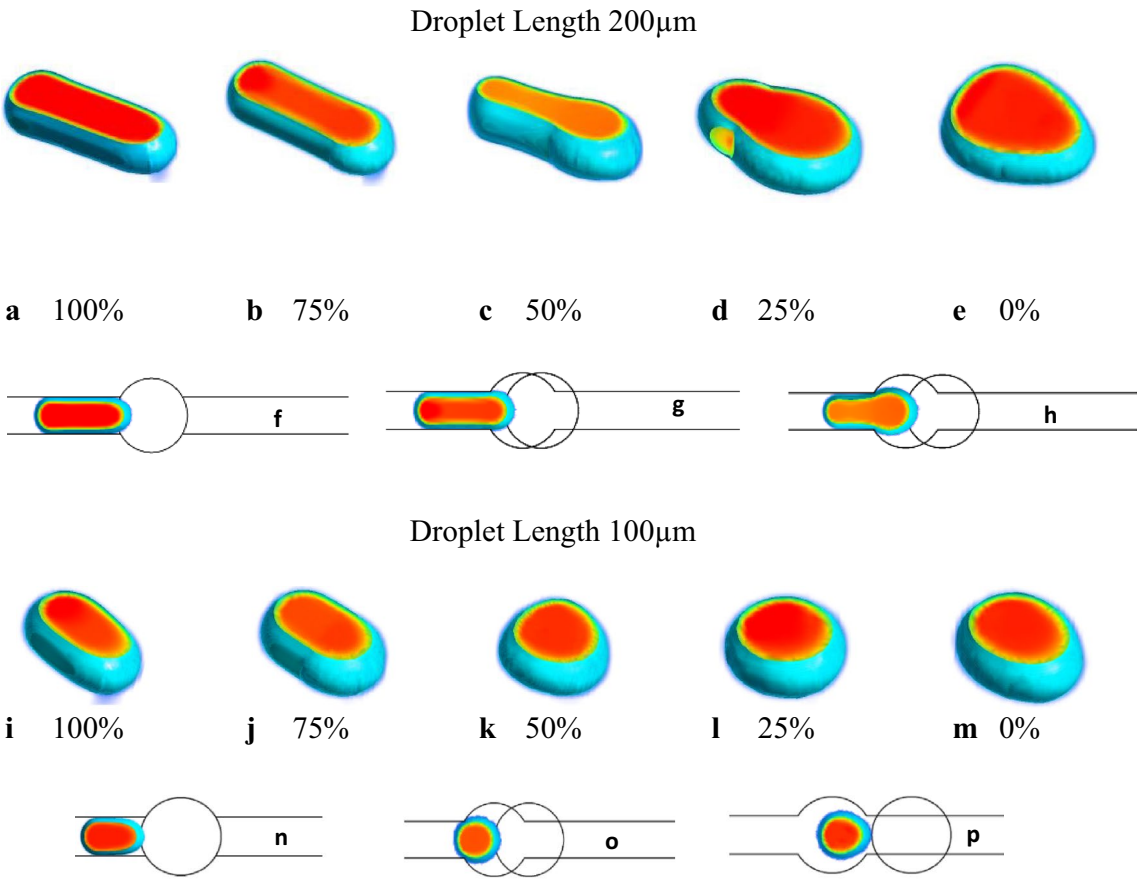

Fig. 7 **a**–**e** Shape of the droplet of different length just before entering the well, for different Pit-Well alignments. **f–h** Top View of droplet motion (length 200 µm) in microchannel before entering the Well, **f** 100% alignment, **g** 75% alignment **h** 50% alignment. **i**–**m** Shape of the droplet (length = 100 µm) just before entering the well, for different Pit-Well alignments. **n**, **p** Top View of droplet motion (length 100 µm) in microchannel before entering the well, **n** 100% alignment **o** 50% alignment **p** 0% alignment

same as reported in the experiment. Our simulation results on the size of the droplet and the frequency of the droplet generation are in good agreement with earlier experiments. It may be noted that the length of the droplet decreases with the rise in the flow rate of the continuous (oil) phase liquid. If the flow rate of the dispersed phase liquid is fixed and for an increased flow rate of the continuous phase liquid, the reduction in the droplet size trend scales as C_a^{-1}, whereas in this case, we also increase the flowrate of dispersed phase liquid to maintain the flowrate ratio Q = 0.5, 0.25 and 0.125. Hence the trend in Fig. 8, the reduction in the droplet size scales as $C_a^{1/4}$ as reported [52].

5 Conclusion

We have carried out numerical simulations to investigate the influence of surfactants on droplet generation and trapping in a T-Junction microfluidic device for capillary number ranging from 0.0028 to 0.02 using the VOF method in ANSYS Fluent software. This range of the capillary number corresponds to the squeezing regime and the Squeezing-to-Dripping transition regime for droplet generation.

Our simulations reveal that in the presence of surfactants the length of the droplet reduces from 192 µm to 148 µm, 228 µm to 196 µm and 296 µm to 268 µm when the surfactant concentration is increased from 0% to 4% for $Q_d/Q_c = 0.2$, 0.4 and 0.8, respectively. The frequency of droplet generation is 4.54 Hz, 3.33 Hz and 2.38 Hz for $(Q_d/Q_c) = 0.2$, 0.4 and 0.8, respectively. Thus, as the flowrate Q_c increases the droplet generation frequency increases significantly. Our simulations also indicate that a rise in the concentration of surfactant by 4%, increases the frequency of droplet generation by 16% at the higher capillary number (C_a = 0.02), whereas, there is only a marginal, or no change, in the squeezing regime ($C_a = 0.0028–0.008$).

The 3D simulations on droplet trapping show that, to successfully trap the droplet in a Well, various factors such as droplet length, its velocity, dimensions of the Well and the Pit, alignment of the Well and the Pit, are important. It is seen that a droplet of length of 200 µm gets trapped in the Well, of volume more than twice the volume of the droplet, if the droplet velocity in the channel exceeds a critical velocity for trapping. The critical velocity U_{cr} depends on the geometry of the Well-Pit combination. For a Well having fixed dimensions (200 µm diameter and 200 µm depth) the critical velocity for trapping remains almost constant (4.5 mm/s) for Pit diameter smaller than the channel width. For Pit diameter larger than the channel diameter, the critical velocity increases significantly (to ~ 7.3 mm/s). More significant than this is the fact that the critical velocity in the absence of a surfactant is ~ 18 mm/s. Clearly, the surfactants cause a drastic change in the droplet trapping mechanism. Further, droplet trapping is seen to depend on the depth of the Well for fixed values of the other device parameters. The droplets get trapped only when the Well depth is more than the channel width, irrespective of the extent of Well alignment with the Pit. If only the Well alignment with the Pit is changed from 0% to 100%, keeping all other parameters fixed, it is seen that, for droplet velocity U_c lower than the critical velocity U_{cr}, the droplet invariably gets trapped in the Well. For $U_c > U_{cr}$, the droplet does not get trapped irrespective of the alignment. Very interestingly, if U_c is close to U_{cr}, it is seen that the droplet gets trapped if the Well-Pit alignment is less than 50% and does not get trapped for alignment above 75%. For alignment between 50 and 80% the droplet gets trapped, but several tiny droplets emerge from the main droplet and flow downstream.

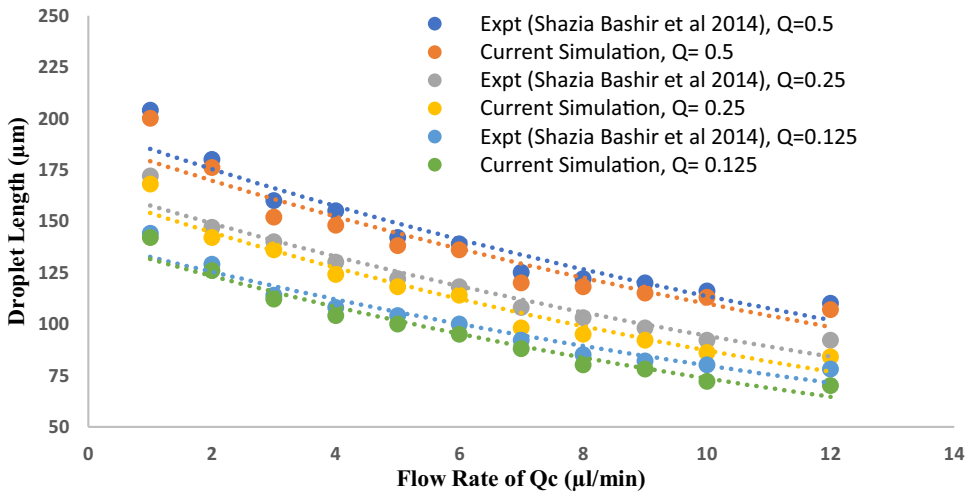

Fig. 8 Droplet length versus Flow rate of the continuous phase liquid (Q_c)

Thus, the escape of the droplet from the Well is often preceded by release of tiny daughter droplets. Our simulation studies have clearly revealed that micro-droplet generation and trapping is a complex phenomenon depending on the device dimensions, fluid properties, surfactant properties and fluid flow parameters. For efficient generation of micro-droplets for a specific application a detailed simulation of the process is essential.

Compliance with ethical standards

Conflict of interest The research carried out does not have any financial obligations or attract any conflict of interest.

References

1. Srinivasan V, Pamula VK, Fair RB (2004) Droplet-based microfluidic lab-on-a-chip for glucose detection. Anal Chim Acta 507:145–150. https://doi.org/10.1016/j.aca.2003.12.030
2. Shui L, Eijkel JCT, van den Berg A (2007) Multiphase flow in microfluidic systems—control and applications of droplets and interfaces. Adv Coll Interface Sci 133:35–49. https://doi.org/10.1016/j.cis.2007.03.001
3. Sun X, Tang K, Smith RD, Kelly RT (2013) Controlled dispensing and mixing of pico- to nanoliter volumes using on-demand droplet-based microfluidics. Microfluid Nanofluid 15:117–126. https://doi.org/10.1007/s10404-012-1133-1
4. Zhu Y, Fang Q (2013) Analytical detection techniques for droplet microfluidics—a review. Anal Chim Acta 787:24–35. https://doi.org/10.1016/j.aca.2013.04.064
5. Vladisavljević GT, Khalid N, Neves MA, Kuroiwa T, Nakajima M, Uemura K, Ichikawa S, Kobayashi I (2013) Industrial lab-on-a-chip: design, applications and scale-up for drug discovery and delivery. Adv Drug Deliv Rev 65:1626–1663. https://doi.org/10.1016/j.addr.2013.07.017
6. Kaler KVIS, Prakash R (2014) Droplet microfluidics for chip-based diagnostics. Sensors 14:23283–23306. https://doi.org/10.3390/s141223283
7. Rakszewska A, Tel J, Chokkalingam V, Huck WT (2014) One drop at a time: toward droplet microfluidics as a versatile tool for single-cell analysis. NPG Asia Mater 6:e133–e133. https://doi.org/10.1038/am.2014.86
8. Schlicht B, Zagnoni M (2015) Droplet-interface-bilayer assays in microfluidic passive networks. Sci Rep 5:1–8. https://doi.org/10.1038/srep09951
9. Ng EX, Miller MA, Jing T, Chen C-H (2016) Single cell multiplexed assay for proteolytic activity using droplet microfluidics. Biosens Bioelectron 81:408–414. https://doi.org/10.1016/j.bios.2016.03.002
10. Hosokawa M, Nishikawa Y, Kogawa M, Takeyama H (2017) Massively parallel whole genome amplification for single-cell sequencing using droplet microfluidics. Sci Rep 7:5199. https://doi.org/10.1038/s41598-017-05436-4
11. Abdollahi P, Karimi-Sabet J, Moosavian MA, Amini Y (2020) Microfluidic solvent extraction of calcium: modeling and optimization of the process variables. Sep Purif Technol 231:115875. https://doi.org/10.1016/j.seppur.2019.115875
12. Mazutis L, Gilbert J, Ung WL, Weitz DA, Griffiths AD, Heyman JA (2013) Single-cell analysis and sorting using droplet-based microfluidics. Nat Protoc 8:870–891. https://doi.org/10.1038/nprot.2013.046
13. Seo M, Paquet C, Nie Z, Xu S, Kumacheva E (2007) Microfluidic consecutive flow-focusing droplet generators. Soft Matter 3:986–992. https://doi.org/10.1039/B700687J
14. Hong Y, Wang F (2007) Flow rate effect on droplet control in a co-flowing microfluidic device. Microfluid Nanofluid 3:341–346. https://doi.org/10.1007/s10404-006-0134-3
15. Li X-B, Li F-C, Yang J-C, Kinoshita H, Oishi M, Oshima M (2012) Study on the mechanism of droplet formation in T-junction microchannel. Chem Eng Sci 69:340–351. https://doi.org/10.1016/j.ces.2011.10.048
16. Sontti SG, Atta A (2017) CFD analysis of microfluidic droplet formation in non–Newtonian liquid. Chem Eng J 330:245–261. https://doi.org/10.1016/j.cej.2017.07.097
17. Han W, Chen X, Hu Z, Yang K (2018) Three-dimensional numerical simulation of a droplet generation in a double T-junction microchannel. JM3 17:025502. https://doi.org/10.1117/1.JMM.17.2.025502
18. Gupta A, Kumar R (2010) Flow regime transition at high capillary numbers in a microfluidic T-Junction: viscosity contrast and geometry effect. Phys Fluids 22:122001. https://doi.org/10.1063/1.3523483
19. Yan Y, Guo D, Wen SZ (2012) Numerical simulation of junction point pressure during droplet formation in a microfluidic T-junction. Chem Eng Sci 84:591–601. https://doi.org/10.1016/j.ces.2012.08.055
20. Glawdel T, Elbuken C, Ren CL (2012) Droplet formation in microfluidic T-junction generators operating in the transitional regime. I. Experimental observations. Phys Rev E 85:016322. https://doi.org/10.1103/PhysRevE.85.016322
21. Carrier O, Funfschilling D, Li HZ (2014) Effect of the fluid injection configuration on droplet size in a microfluidic T junction. Phys Rev E 89:013003. https://doi.org/10.1103/PhysRevE.89.013003
22. Nekouei M, Vanapalli SA (2017) Volume-of-fluid simulations in microfluidic T-junction devices: influence of viscosity ratio on droplet size. Phys Fluids 29:032007. https://doi.org/10.1063/1.4978801
23. Marsousi S, Karimi-Sabet J, Moosavian MA, Amini Y (2019) Liquid-liquid extraction of calcium using ionic liquids in spiral microfluidics. Chem Eng J 356:492–505. https://doi.org/10.1016/j.cej.2018.09.030
24. Tadros TF (2013) Emulsion formation, stability, and rheology. In: Emulsion formation and stability. John Wiley & Sons, Ltd, New Jersey pp 1–75
25. Peng L, Yang M, Guo S, Liu W, Zhao X (2011) The effect of interfacial tension on droplet formation in flow-focusing microfluidic device. Biomed Microdevices 13:559–564. https://doi.org/10.1007/s10544-011-9526-6
26. Han W, Chen X (2019) New insights into the pressure during the merged droplet formation in the squeezing time. Chem Eng Res Des 145:213–225. https://doi.org/10.1016/j.cherd.2019.03.002
27. Bashir S, Rees JM, Zimmerman WB (2011) Simulations of microfluidic droplet formation using the two-phase level set method. Chem Eng Sci 66:4733–4741. https://doi.org/10.1016/j.ces.2011.06.034
28. Glawdel T, Ren CL (2012) Droplet formation in microfluidic T-junction generators operating in the transitional regime. III. Dynamic surfactant effects. Phys Rev E 86:026308. https://doi.org/10.1103/PhysRevE.86.026308
29. Wang R (2013) Nanoparticles influence droplet formation in a T-shaped microfluidic. J Nanopart Res 15:2128. https://doi.org/10.1007/s11051-013-2128-x
30. Wehking JD, Gabany M, Chew L, Kumar R (2014) Effects of viscosity, interfacial tension, and flow geometry on droplet

formation in a microfluidic T-junction. Microfluid Nanofluid 16:441–453. https://doi.org/10.1007/s10404-013-1239-0
31. Bastani D, Fayzi P, Lotfi M, Arzideh SM (2018) CFD simulation of bubble in flow field: investigation of dynamic interfacial behaviour in presence of surfactant molecules. Colloid Interface Sci Commun 27:1–10. https://doi.org/10.1016/j.colcom.2018.09.001
32. Riaud A, Zhang H, Wang X, Wang K, Luo G (2018) Numerical study of surfactant dynamics during emulsification in a T-Junction microchannel. Langmuir 34:4980–4990. https://doi.org/10.1021/acs.langmuir.8b00123
33. Wang K, Zhang L, Zhang W, Luo G (2016) Mass-transfer-controlled dynamic interfacial tension in microfluidic emulsification processes. Langmuir 32:3174–3185. https://doi.org/10.1021/acs.langmuir.6b00271
34. Dangla R, Lee S, Baroud CN (2011) Trapping microfluidic drops in wells of surface energy. Phys Rev Lett 107:124501. https://doi.org/10.1103/PhysRevLett.107.124501
35. Wang W, Yang C, Li CM (2009) On-demand microfluidic droplet trapping and fusion for on-chip static droplet assays. Lab Chip 9:1504–1506. https://doi.org/10.1039/B903468D
36. Simon MG, Lin R, Fisher JS, Lee AP (2012) A Laplace pressure based microfluidic trap for passive droplet trapping and controlled release. Biomicrofluidics 6:014110. https://doi.org/10.1063/1.3687400
37. Abbyad P, Dangla R, Alexandrou A, Baroud CN (2011) Rails and anchors: guiding and trapping droplet microreactors in two dimensions. Lab Chip 11:813–821. https://doi.org/10.1039/C0LC00104J
38. Nagel M, Brun P-T, Gallaire F (2014) A numerical study of droplet trapping in microfluidic devices. Phys Fluids 26:032002. https://doi.org/10.1063/1.4867251
39. Amselem G, Brun PT, Gallaire F, Baroud CN (2015) Breaking anchored droplets in a microfluidic Hele-Shaw Cell. Phys Rev Applied 3:054006. https://doi.org/10.1103/PhysRevApplied.3.054006
40. Liu H, Zhang Y (2017) Lattice Boltzmann simulation of the trapping of a microdroplet in a well of surface energy. Comput Fluids 155:68–75. https://doi.org/10.1016/j.compfluid.2016.10.031
41. Soh GY, Yeoh GH, Timchenko V (2016) Improved volume-of-fluid (VOF) model for predictions of velocity fields and droplet lengths in microchannels. Flow Meas Instrum 51:105–115. https://doi.org/10.1016/j.flowmeasinst.2016.09.004
42. Li L, Karymov MA, Nichols KP, Ismagilov RF (2010) Dead-end filling of slipchip evaluated theoretically and experimentally as a function of the surface chemistry and the gap size between the plates for lubricated and dry SlipChips. Langmuir 26:12465–12471. https://doi.org/10.1021/la101460z
43. Vivek Ranade (2019) Computational Flow Modeling for Chemical Reactor Engineering, vol 5, 1st Edn. https://www.elsevier.com/books/computational-flow-modeling-for-chemical-reactor-engineering/ranade/978-0-12-576960-0. Accessed 24 Nov 2019
44. Brackbill JU, Kothe DB, Zemach C (1992) A continuum method for modeling surface tension. J Comput Phys 100:335–354. https://doi.org/10.1016/0021-9991(92)90240-Y
45. Bashir S, i Solvas XC, Bashir M, Rees JM, Zimmerman WBJ (2014) Dynamic wetting in microfluidic droplet formation. BioChip J 8:122–128. https://doi.org/10.1007/s13206-014-8207-y
46. Garstecki P, Fuerstman MJ, Stone HA, Whitesides GM (2006) Formation of droplets and bubbles in a microfluidic T-junction—scaling and mechanism of break-up. Lab Chip 6:437–446. https://doi.org/10.1039/B510841A
47. Kagawa Y, Ishigami T, Hayashi K, Fuse H, Mino Y, Matsuyama H (2014) Permeation of concentrated oil-in-water emulsions through a membrane pore: numerical simulation using a coupled level set and the volume-of-fluid method. Soft Matter 10:7985–7992. https://doi.org/10.1039/C4SM00705K
48. Menech MD, Garstecki P, Jousse F, Stone HA (2008) Transition from squeezing to dripping in a microfluidic T-shaped junction. J Fluid Mech 595:141–161. https://doi.org/10.1017/S002211200700910X
49. Abate AR, Mary P, van Steijn V, Weitz DA (2012) Experimental validation of plugging during drop formation in a T-junction. Lab Chip 12:1516–1521. https://doi.org/10.1039/C2LC21263C
50. Kovalchuk NM, Roumpea E, Nowak E, Chinaud M, Angeli P, Simmons MJH (2018) Effect of surfactant on emulsification in microchannels. Chem Eng Sci 176:139–152. https://doi.org/10.1016/j.ces.2017.10.026
51. Li G, Chen Q, Li J, Jianlong Z (2009) Optimization of surface-tension-induced droplet trapping for static mi-croarray applications. In: Thirteenth international conference on miniaturised systems for chemistry and life science, Nov 1–5, 2009, Jeju, Korea, 978-0-9798064-2-1/μTAS2009/$20©2009CBMS
52. van der Graaf S, Nisisako T, Schroën CGPH, van der Sman RGM, Boom RM (2006) Lattice Boltzmann simulations of droplet formation in a T-shaped microchannel. Langmuir 22:4144–4152. https://doi.org/10.1021/la052682f